SURFACE-FLUCTUATIONS ON CLATHRATE HYDRATE STRUCTURE I AND II SLABS IN SELECTED ENVIRONMENTS

Bjørn Steen Sæthre*, Alex C. Hoffmann
Dept. of Physics and Technology
University of Bergen
Allegaten 55, 5007 Bergen
NORWAY

ABSTRACT

Hydrates in some crude oils have a smaller tendency to form plugs than in others, and lately this is becoming a focus of research. To study this and the action of hydrate antiagglomerants in general, hydrate surface properties must be known. To help in characterizing the surface properties by simulation, the capillary waves of clathrate hydrate surfaces in vacuum are examined in all unique crystal faces by Molecular Dynamics, and an attempt is made to estimate the surface energies in the respective crystal faces from the wave fluctuations [1]. We also attempt to estimate solid/liquid surface energies of hydrate/oil and hydrate/water for a specific face, for comparison. The forcefield OPLS_AA is used for the organic compounds, while TIP4P/ice is used for the water framework. The anisotropy of the surface energy is then estimated and the result compared to the initial growth rate of different crystal faces as found in experiment. [2]

Keywords: gas hydrates, plug prevention, surface energy, molecular dynamics

LIST OF SYMBOLS

Symbol	Definition
a	Capillary length [m]
A	Interfacial area [nm^2]
c_1 c_2	Cubic harmonic exp. coeff. [-]
g	Gravitational acceleration [m/s^2]
$\mathcal{H}[z]$	Hamiltonian of $z[\mathbf{r}]$ [kJ/mol]
k_B	Boltzmann constant [J/K]
k, k_i	wavenumber [nm^{-1}]
l	Min. surface wavelength [nm]
L	Max. surface wavelength [nm]
p	Pressure [Bar]
P	Probability [-]
R^2	Sample correlation coeff.[-]
$\mathbf{s}_{ij}$	(Surface) stress tensor [mN/m]
dS	Element of surface [nm^2]
T	Temperature [K]
V	Volume [nm^3]
$\mathbf{r}$	$= (x, y)$ surface coordinates
$\langle X \rangle$	Average of X
$z(x, y)$	Model for real interface
α	Fourier expansion coefficient
γ	Surface free energy
κ	Interfacial stiffness [mN/m]
ϵ	(Surface) Strain tensor
μ	Chemical potential [kJ/mol]
ρ	Density [kg/m^3]
θ	Angle
(xyz)	Normal to 1D-strip
$[uvw]$	Tangent to 1D-strip

INTRODUCTION

Hydrates formed by water and light hydrocarbon molecules are increasingly becoming the focus of research in the energy industries and academia.

One reason for this is that the energy in-

*Corresponding author: Phone: +47 55 582869 Fax: +47 55 589440 E-mail: bjorn.sathre@ift.uib.no

dustry is becoming aware of the potential energy resource that naturally occurring hydrate reservoirs constitute, and methods for extracting methane from such reservoirs are being sought [3–9].

Another reason, which is the focus of this paper, is that plugging of pipelines, particularly subsea pipelines, by hydrates is becoming an increasingly costly problem. As oil and gas exploration is expanding into the arctic regions, conditions in subsea pipelines are getting further into the hydrate-stable region, giving rise to extra costs in hydrate prevention.

While natural hydrate reservoirs often contain almost pure methane, and therefore mainly are structure I, hydrates in pipelines form in the presence of a variety of light hydrocarbons, and are therefore often structure II, since this is the thermodynamically favored configuration in all but the purest methane gas environments [10].

At present, thermodynamic inhibitors are added, often in large amounts [11], to avoid plugging by pipeline hydrates. In the HYPERION project, of which this study is a part, the focus is on managing the risk of plug formation in the presence of hydrate particles, rather than on suppressing hydrate particle formation in the first place. This is a relatively new focus in hydrate research [12]. In this field of study, quantification of the plugging tendency of hydrate particles in various pipeline-liquid environments is important, as is the identification of anti-agglomerants for hydrates and the issue of why some oils tend to form plugs under hydrate-stable conditions and others not [13–17]. This latter is thought to be related to the occurrence in some oils of natural inhibiting components (NICs).

In this approach to hydrate management, the cohesivity of hydrate particles, and therefore their surface energy, in the presence of various pipe-line liquids and also in the presence of a variety of trace components, potentially acting as anti-agglomerants, is crucial.

The surface energy of hydrates is also needed to predict the rate of growth of hydrate particles, and knowing the difference between the surface energies on the crystal faces aids in predicting the shape of the particles formed, which may again impact the formation of hydrate plugs.

In this paper, surface energies of hydrates are studied using classical Molecular Dynamics.

THEORY

It is well known that the surface free-energy of interfaces with elastic solids is not in general equal to the interfacial stress (or the measured surface tension of contacting fluids). This is due to the fact that the surface of solids, in contrast to that of liquids, can deform, e.g. expand, by elastic deformation, accumulating shear stress but without exposing more particles (atoms, ions or molecules) from bulk to the surface.

Mathematically this is embodied in the Shuttleworth relation [18].

$$\mathbf{s}_{ij} = \gamma\delta^i_j + \left(\frac{\partial\gamma}{\partial\epsilon}\right)_{T,V,\mu} \tag{1}$$

This necessitates another route to the surface-free energy of solid-fluid interfaces than the conventional method used for fluids, i.e. calculating the difference between the normal and tangential components of the stress tensor, which only works for solids in the absence of elastic stresses in the surface. This latter condition is near impossible to achieve in the small timespans and spatial scales of molecular modelling.

Capillary wave fluctuations and their relation to interfacial stiffness

We can overcome the difficulties presented by possible elastic stress by modelling the interface as a fluctuating membrane according to the theory of capillary waves [19,20]. We consider the interface as a mathematical 2D surface $z = z(\mathbf{r}) = z(x, y)$. The Hamiltonian is:

$$\mathcal{H}[z(\mathbf{r})] = \iint_A \mathbf{dS}\left(\kappa\sqrt{1+(\nabla z(\mathbf{r}))^2} + \int_0^z dh\,\Delta\rho g h\right) \tag{2}$$

The Hamiltonian functional contains two terms, the first comes from the work of creating surface by extending the membrane, and the second term comes from the work against gravity. This second term is only needed for obtaining an analytic solution to the problem, and will be removed by a limiting procedure in our case of zero gravity. κ is the interfacial stiffness, and $\Delta\rho$ is the density difference between the phases separated by the interface. We can linearize Eq. (2) into:

$$\mathcal{H}[z(\mathbf{r})] = \iint_A \mathbf{dS}\,\left(\kappa\,(1+\frac{1}{2}(\nabla z)^2)+\frac{1}{2}\Delta\rho g z^2\right) \quad (3)$$

This is to be examined under the periodic boundary conditions in the simulation box:

$$z(0,y)=z(L,y) \quad z(x,0)=z(x,L) \quad (4)$$

Now we perform a spectral analysis of the energy functional. To that end we consider the possible discrete oscillation modes of the periodic surface:

$$z[\mathbf{k}] = \sum_{\mathbf{k}} \alpha(\mathbf{k}) e^{i\mathbf{k}\cdot\mathbf{r}} \quad (5)$$

By substituting Eq. (5) in Eq. (3) and using the known relation for the Fourier transform of the derivative, we obtain:

$$\mathcal{H}[z(\mathbf{k})] = \kappa A + \frac{1}{2}\kappa A \sum_{k_x}\sum_{k_y} \alpha(k_x)\alpha(k_y) \left(\int_x\int_y \mathbf{dS}\, e^{i(k_x x+k_y y)}(2a^{-2}-k_x k_y)\right) \quad (6)$$

Where a is a generalized capillary length, $a^2 = 2\kappa/(\Delta\rho g)$

Imposing the boundary conditions, Eqs. (4), k_x and k_y have the allowed values $2\pi n/L$, $n \in \mathbf{Z}$. With the above boundary conditions, the functional vanishes for all k_x,k_y unless $k_x = -k_y$. This gives the following energy spectrum upon integration:

$$\mathcal{H}[z[k]] = \kappa A(1+\frac{1}{2}\sum_k (\alpha(k)\alpha(-k) \times (2a^-2+k^2)) \quad (7)$$

where k is the absolute value of k_x and k_y.

The mean square fluctuations of the interface position for a given set of modes are:

$$\langle z^2\rangle = A^{-1}\iint_A z^2(\mathbf{r})\mathbf{dS} = \sum_{k>0}\alpha(k)\alpha(-k) \quad (8)$$

where the last equality comes from the well-known Parseval's relation.

Now, the probability of finding a mode with energy $E[k]$ in the canonical ensemble is

$$\mathrm{P} \propto e^{-\frac{H[z[k]]}{k_B T}}$$

In our linear approximation it means that the spectrum of modes has a Normal distribution. >From the properties of the Normal distribution we know that the expectation value of a squared Normal variable (in our case z^2) is equal to the Variance of the Normal distribution. The variance can be easily read off the Normal probability density function as the quadratic part of $\mathrm{P}[H[k]]$. That is, the expected fluctuations in our linearized model become:

$$\langle z^2\rangle = \sum_{k>k_{min}}\langle\alpha(k)\alpha(-k)\rangle = \frac{k_B T}{\kappa A}\sum_{k>0}\frac{1}{2a^{-2}+k^2} \quad (9)$$

Obviously the dominant contribution to the expectation value comes from the low-wavenumber ripples, which the boundary conditions dictate to be $k_{min} = 2\pi/L$. The maximum wavenumber is more challenging to connect to a measurable quantity, but it has to be an integer multiple of k_{min}, let us say $k_{max} = 2\pi/l$ where l is a length of molecular dimensions.

Transferring to a circular cut-off in 2D wave-vector space, and using the continuum approximation we have: $\sum_{k=k_{min}}^{k_{max}} \mapsto \int_{k_{min}}^{k_{max}} k/(2\pi)\,dk$. Integrating equation (9) out we arrive at the following expression

$$\langle z^2\rangle = \frac{k_B T}{4\pi\kappa}\ln\left[\frac{1+2(\pi a/l)^2}{1+2(\pi a/L)^2}\right]$$

. where l corresponds to the minimum, and L to the maximum lengthscale of capillary waves respectively. Now letting gravity: $g \to 0$, the capillary length goes to infinity, and the expression above becomes:

$$\langle z^2 \rangle = \frac{k_B T}{4\pi\kappa} \ln\left[\frac{L^2}{l^2}\right] = \frac{k_B T}{2\pi\kappa} \ln\left[\frac{L}{l}\right]. \quad (10)$$

In case of a 1D strip, the derivation is similar, and the result is [20]:

$$\langle z^2 \rangle = \frac{1}{\sqrt{2}\pi^2} \frac{k_B T}{\kappa} L(1 - O[l/L]). \quad (11)$$

As can be seen the fluctuation scales linearly with the linear size of the system in this case, as opposed to logarithmically which would lead to larger signal-to-noise ratio. This, and the singling out of a preferred direction on the surface (see next section), is the main reason for adopting this geometry.

On interfacial stiffness and surface free energy and a means to decouple them

As noted above, both surface stiffness and surface free energy in elastic materials are direction dependent. The fluctuation spectrum therefore depends not only on the magnitude of γ. but also on the energy required for local orientation-fluctuations. [21] The anisotropy can be quantified with the help of the parameter θ, defined to be the angle between the instantaneous face normal, and the normal of a crystallographic reference face. The surface stiffness $\kappa(\theta)$ is then related to the surface free energy $\gamma(\theta)$ through

$$\kappa(\theta) = \gamma(\theta) + \frac{d^2\gamma}{d\theta^2} \quad (12)$$

To decouple the interfacial free energy γ from the surface stiffness κ we have to measure the stiffness in several different interfacial orientations, and the free energy can then be determined indirectly if we can fit $\gamma(\theta)$ to a suitable function describing the fluctuation anisotropy. Such a function must conform to the symmetries of the crystal. As hydrates have cubic symmetry, a natural choice would be cubic harmonics. Like Davidchack et. al. [22] we start with the product expansion [23]:

$$\frac{\gamma(\mathbf{n})}{\overline{\gamma}} = c_1 \left(\sum_i n_i^4 - \frac{3}{5} \right) + c_2 \left(3\sum_i n_i^4 + 66(n_1 n_2 n_3)^2 - \frac{17}{7} \right) \quad (13)$$

where c_1 and c_2 are expansion coefficients capturing the anisotropy.

We see that we have 3 undetermined parameters, $\overline{\gamma}$, c_1, and c_2. To fix these we need to measure the surface fluctuations in at least the 3 unique faces: (001), (110) and (111) of the crystal, preferably we should overdetermine the system by measuring fluctuations in more than one direction on each face.

We obtain the following formulas for the directional interfacial free energy and stiffness in terms of the averaged interfacial free energy and the anisotropy parameters c_1 and c_2 [22] (Observe that we differ by using the tangent-vector and not the binormal-vector for the surface strip as reference):

(Face)[t]	$\frac{\gamma}{\overline{\gamma}}$	$\frac{\kappa}{\overline{\gamma}}$
(001)[100], [010]	$1 + \frac{2}{5}c_1 + \frac{4}{7}c_2$	$1 - \frac{18}{5}c_1 - \frac{80}{7}c_2$
(110)[1$\overline{1}$0]	$1 - \frac{1}{10}c_1 - \frac{13}{14}c_2$	$1 + \frac{39}{10}c_1 + \frac{155}{14}c_2$
(110[001]	$1 - \frac{1}{10}c_1 - \frac{13}{14}c_2$	$1 - \frac{21}{10}c_1 + \frac{365}{14}c_2$
(111)[11$\overline{2}$]	$1 - \frac{4}{15}c_1 + \frac{64}{63}c_2$	$1 + \frac{12}{5}c_1 - \frac{1280}{63}c_2$

METHOD

We perform a series of Molecular Dynamics simulations over $O(10^6)$ steps with a system size of $O(10000)$ atoms. Constructing the clathrate hydrates structure I and II, we follow the procedure outlined in our previous work [24] employing the space groups Pm3n and Fd3m for respectively structure I and II hydrate.

Our setup conforms essentially to that of Davidchack et. al [22]. However, we employ a slightly different analysis—measuring density-profiles and direct fluctuations in real space (Eq. 10) and furthermore we also compare with measurements using the full 2D model. Since we do not have a truly 1D system, we found it suitable to employ a purely

2D analysis, even when our pseudo-1D geometry were adopted to enhance the surface-wave fluctuations over the bulk fluctuations. To decouple the free energy from the measured surface stiffness we perform vacuum simulations of the hydrate slabs. We then use the vacuum simulations to calibrate the geometric direction-dependent factors of the cubic harmonic expansion for our particular geometry. Having obtained the cubic harmonic expansion, we can then directly convert the hydrate/fluid interfacial stiffnesses to surface energy values. Since we are only able to do this rigorously for the pseudo-1D surface geometry at present. We can only give interfacial stiffnesses for the 2D simulations.

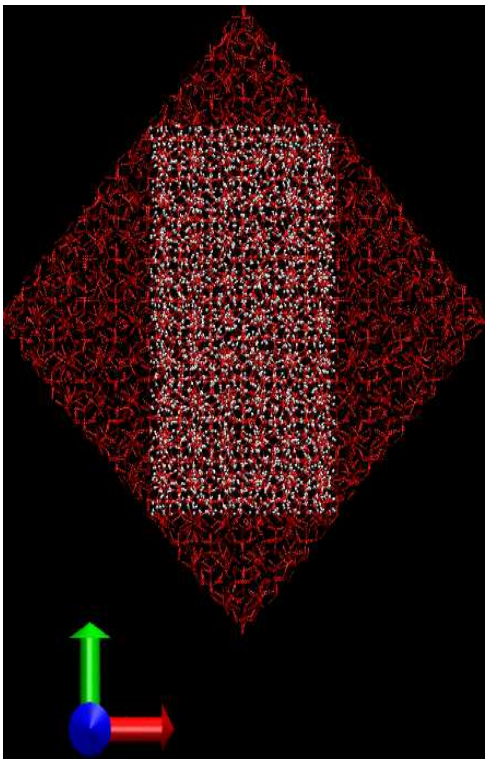

Figure 1: Construction (110)-face - hydrate II

The protocol is as follows:

Geometric construction We replicate and stack the unit cell to a large cube, then rotate the crystal, so that each of the planes (100) (110) and (111) are successively brought into alignment with the xy-plane of the simulation box to make three separate starting configurations.

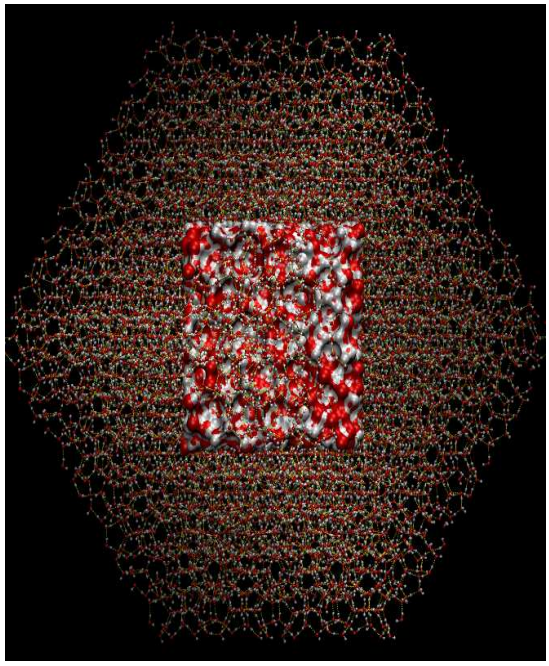

Figure 2: Construction (111) - face - hydrate II

Clipping - 2D We crop the start-up configurations prepared above by planar cuts to make an elongated rectangular prism with square cross section in the Z-direction of the simulation box. The cuts are not sharp, no molecules are split up.

Clipping - 1D We crop the start-up configurations in a preferred direction, making a strip of surface

Energy minimization A brief steepest descent minimization was used to correct for edge-effects

Equilibration We equilibrate the systems using the Berendsen thermostat and barostat [25]. The pressure scaling is done with independent box scaling in the 3 orthogonal coordinate directions.

Vacuum or fluid addition - We expand the box in the z-direction to create roughly 1/3 of total volume to be filled with vacuum, or one of the process fluids to be investigated.

Production simulations The production runs are performed in the NVT-ensemble

using the Noose-Hoover thermostat. [26]

Analysis We fit the interfacial density-profile of waters averaged over the whole trajectory to the expected Gaussian form in capillary wave-theory [27]:

$$\rho(z) = 1/2 \times (\rho_1 + \rho_2) -$$
$$1/2 \times (\rho_1 - \rho_2) \times erf\left((z - h_0)/\sqrt{2\langle z^2 \rangle}\right)$$

We extract the thickness from the average of our two equivalent interfaces.

The details of the general MD technicalities (treatment of cut-offs, neighbourlists, electrostatics and constraints) are given in table 4

Parameters used in the energy minimization and equilibration are given in tables 2 and 3 respectively.

Table 1: General MD parameters

Neighboursearch & PBC	
Algorithm	Verlet list [28]
Verlet list cut-off	0.9 nm
Update freq.	5 steps
PBC	all directions
Electrostatics & vdW	
Electrostatics	PME [29]
PME interpol. order	5
FFT-grid spacing	$\sim$ 0.1nm
Ewald sum dir./recip.	10^{-5}
vdW. force	Twin range cut-off
neigbourlist-cutoff	0.9 nm
vdW cut-off upper	1.4 nm
Bond constraints	
Constraints	All bond lengths
Algorithm - Waters	SETTLE [30]
SETTLE parameters	(TIP4P/ice model)
Algorithm - Others	LINCS [31]
LINCS order	4
LINCS Iter. - SIM.	1
LINCS Iter. - EM	6

ANALYSIS AND RESULTS

The setups of the surface fluctuation simulations are given in tables 5 and 6.

Table 2: Energy minimization parameters

Algorithm	Steepest-descent
Steps	300
Maximum step-size	0.1 nm
Tolerance	25 kJ (mol nm)$^{-1}$

Table 3: Equilibration parameters

Molecular Simulation	
Algorithm	Leap-frog(Vel. Verlet)
EQ steps	50000
Stepsize	2 fs
Center of mass motion removal	
Type	Trans'l momentum
Frequency	Every step
Recording periods	
Coordinate	500 steps (1 ps)
Velocity	5000 steps (10 ps)
Force	5000steps (10 ps)
Energy	10 steps (0.02 ps)
Thermostat	
Algorithm	Berendsen
Coupling time	0.1 ps
Range	All molecules
Barostat	
Algorithm	Berendsen
Coupling time	0.5 ps
Init. compressibility	4×10^{-5} Bar^{-1}

The fluctuations obtained by fitting to density profiles are given in tables 7 and 8 and the profiles for structure II are graphed in figure 4 for the pseudo-1D geometry. The profiles were obtained by dividing the box, normally of length $\approx$10nm, into 1000 bins to obtain a binwidth of 0.01 nm.

We see that our present simulations are plagued by quite large uncertainties with this methodology, showing the urgent need for a rigorous, more precise way to define the extent and position of the interface, or alternatively for studying the profile's development in time. We are still able to make some qualitative inferences from the pseudo-1D simu-

Table 4: Simulation parameters

Molecular Simulation	
Algorithm	Leap-frog (Vel. Verlet)
EQ steps	5×10^6
Stepsize	2 fs
Recording periods	
Coordinate	1000 steps (2 ps)
Velocity	10000 steps (20 ps)
Force	10^5 steps (200 ps)
Energy	500 steps (1 ps)
Thermostat	
Algorithm	Nose-Hoover [26]
Coupling time	0.1 ps
Range	All molecules

Table 5: Simulation matrix—Pseudo 1D geom., hydrate/vacuum

Hyd.	(Face)[s]	Box [nm]	No.
HI	(001)[010]	2.88×7.27×10.8	19224
HI	(110)[-110]	5.99×3.10×9.00	12233
HI	(111)[11-2]	6.98×3.10×10.5	14116
HII	(001)[100]	6.92×3.45×10.3	15168
HII	(110)[001]	3.11×6.08×9.50	14751
HII	(110)[-110]	6.97×3.15×10.0	18289
HII	(111)[11-2]	3.22×6.05×12.1	14675

lations. Expanding the stiffnesses in cubical harmonics we estimate the surface energies in the pseudo 1D geometry, shown along with the surface stress in table 9.

Having obtained the expansion parameters of the cubic-harmonic expansion from the pseudo-1D fit, we now utilize it to crudely estimate the surface energies of the structure II hydrate (001)-face with the fluid phases from the stiffnesses obtained in the the 2D simulation results in table 10.

DISCUSSION

First we note that in all our simulations there is not an obvious relation between the surface stresses, obtained from the fluid-fluid approximation, and the surface energies as inferred via surface-stiffness measurements us-

Table 6: Simulation matrix—2D geom, hydrate/vacuum.

System	(Face)	Box [nm]	No.
HII/vac	(001)	3.40×3.40×10.0	10112
HII/vac	(110)	3.54×3.45×10.2	9783
HII/vac	(111)	3.56×3.49×10.5	10923
HII/wat	(001)	3.42×3.45×6.34	9854
HII/oil	(001)	3.37×3.37×8.22	10672
HI/vac	(001)	3.60×3.61×10.7	12096
HI/vac	(110)	3.68×3.57×10.9	12390
HI/vac	(111)	3.68×3.71×10.9	12824

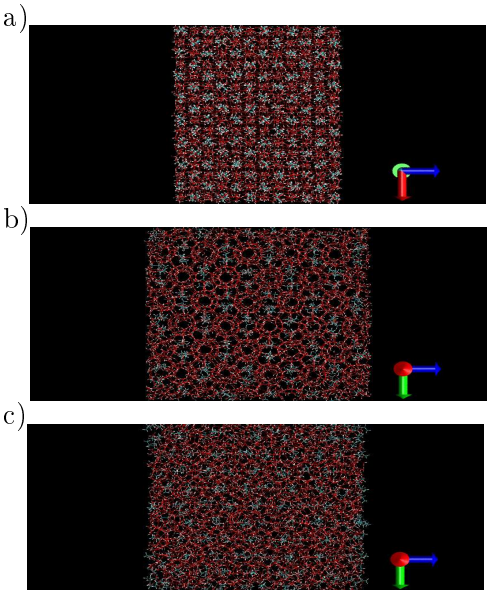

Figure 3: Hydrate II/vacuum strip configuration - a) (001)[100], b) (110)[001], c) (111)[-110]

ing capillary wave theory. By construction we do not see negative values for the surface energy, as we do with stresses. It is seen that the values of surface tension for structure II hydrate conforms qualitatively to the experimentally determined relation between the growth rate of faces in the structure II crystal [2]: (100)>(110)>(111), however our results are mostly forced by the fit to the cubic harmonics and therefore not well established yet, since the uncertainties are substantial. Furthermore, only the relative values can be said to have importance since we have employed an ad-hoc assumption of minimum wavelength-

Table 7: Surface fluctuations from density profiles—pseudo-1D strip

Interface	T [K]	p. [Bar]	Fluct. [10^{-3}nm^2]	κ [mN/m]
Hydrate I / vacuum				
(001)[010]	254	10	7.6(1.8)	155(40)
(110)[-110]	254	10	8(1.5)	140(30)
(111)[11-2]	254	10	11(2)	103(17)
Hydrate II / vacuum				
(100)[001]	254	3	4.9(5)	253(8)
(110)[001]	254	3	8.2(3)	127(4)
(110)[-110]	254	3	8.1(1)	138(2)
(111)[11-2]	254	3	37(13)	28(10)

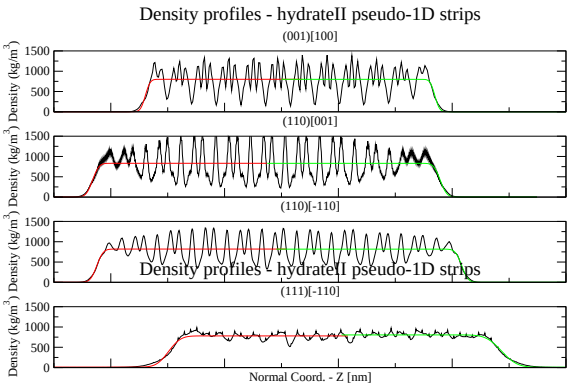

Figure 4: Density profiles - Hydrate II strips/vacuum (Water framework only)

cutoff being of the order of the largest-cage diameter in our hydrate structure. (We have as yet not been able to estimate the bulk-correlation length in hydrates from our simulations.) In the both cases the results are numerically somewhat large, and for structure I up to now all too uncertain to make any inferences of ordering. As seen from the above the results for structure I do not at all conform to the results of Smelik et. al: [2] which confirms our reservations as to the uncertainties inherent in the present method of analysis. Although our method shows a greater affinity for hydrate to the water phase than to the oil phase. The magnitude of the interaction with water is quite hard to ascertain due to the smooth transition to the water phase seen in density profiles. Especially after long simulation times the hydrate water-structure is con-

Table 8: Surface fluctuations from density profiles—2D geometry

(Face)	T. [K]	p. [Bar]	Fluct. [10^{-3}nm^2]	κ [mN/m]
Hydrate I / vacuum				
(001)	254	10	5(4)	160(150)
(110)	254	10	11(4)	80(30)
(111)	254	10	13(2)	61(9)
Hydrate II / vacuum				
(001)	254	3	5.8(0.5)	124(12)
(110)	254	3	8(1)	93(13)
(111)	254	3	7.4(0.3)	103(4)
Hydrate II				
(001)/oil	253	2	7.7(0.2)	92(18)
(001)/wat	253	2	2.9(1.7)	24(12)

Table 9: Surface energies—hydrates—pseudo 1D strips

System	Face (Index)	T [K]	γ [mN/m]	Stress [mN/m]
HI/vac	(001)	254	147	56.3(4)
HI/vac	(110)	254	148	-43.2(4)
HI/vac	(111)	254	152	42.1(4)
γ_{avg}			149	
HII/vac	(001)	254	133	92(1)
HII/vac	(110)	254	141	101.4(5)
HII/vac	(111)	254	144	66(1)
γ_{avg}			140(60)	

Table 10: Surface energies—hydrate/fluids—2D slabs

System	T [K]	γ [mN/m]	Stress [mN/m]
HII/vacuum	254	139(60)	-443(2)
HII/oil	254	65(13)	-198(2)
HII/water	254	17(8)	-17(1)

tinued in ordered water-clusters, and a clear identification of the profile thus becomes difficult. Surface energy for the hydrate/water interface in our simulation is therefore near negligible, due to the smoothness of the density transition. Implementing an order parameter for solid phases of water, to more precisely determine the position and extent of the interface, would be of great help in reducing the main source of uncertainty in the method.

REFERENCES

[1] J. J. Hoyt, M. Asta, and A. Karma. *Method for computing the anisotropy of the solid-liquid interfacial free energy.* Physical Review Letters 2001;86(24):5530–5533.

[2] E. A. Smelik and H. E. King. *Crystal-growth studies of natural gas clathrate hydrates using a pressurized optical cell.* American Mineralogist 1997;82(1-2):88–98.

[3] B. Kvamme, A. Graue, E. Aspenes, T. Kuznetsova, L. Granasy, G. Toth, T. Pusztai, and G. Tegze. *Kinetics of solid hydrate formation by carbon dioxide: Phase field theory of hydrate nucleation and magnetic resonance imaging.* Physical Chemistry Chemical Physics 2004;6:2327–2334.

[4] A. V. Milkov. *Global estimates of hydrate-bound gas in marine sediments: how much is really out there?* Earth-Science Reviews 2004;66:183–197.

[5] R. Boswell. *Resource potential of methane hydrate coming into focus.* Journal of Petroleum Science and Engineering 2007;56:9–13.

[6] M. J. Castaldi, Y. Zhou, and T. M. Yegulalp. *Down-hole combustion method for gas production from methane hydrates.* Journal of Petroleum Science and Engineering 2007;56:176–185.

[7] R. A. Dawe and S. Thomas. *A large potential methane source - natural gas hydrates.* Energy Sources Part A-Recovery Utilization and Environmental Effects 2007;29:217–229.

[8] K. W. Jones, P. B. Kerkar, D. Mahajan, W. B. Lindquist, and H. Feng. *Microstructure of natural hydrate host sediments.* Nuclear Instruments & Methods in Physics Research Section B-Beam Interactions with Materials and Atoms 2007;261:504–507.

[9] I. N. Tsimpanogiannis and P. C. Lichtner. *Parametric study of methane hydrate dissociation in oceanic sediments driven by thermal stimulation.* Journal of Petroleum Science and Engineering 2007;56:165–175.

[10] A. L. Ballard. *Hydrate phase diagrams for methane plus ethane plus propane mixtures.* Chemical Engineering Science 2001;56(24):6883–6895. 0009-2509.

[11] J. D. Lee, R. Susilo, and P. Englezos. *Methane-ethane and methane-propane hydrate formation and decomposition on water droplets.* Chemical Engineering Science 2005;60(15):4203–4212.

[12] E. D. Sloan. *A changing hydrate paradigm—from apprehension to avoidance to risk management.* Fluid Phase Equilibria 2005;228–229:67–74.

[13] F. H. Fadnes. *Natural hydrate inhibiting components in crude oils.* Fluid Phase Equilibria 1996;117(1-2):186–192.

[14] L. Bergflodt, L. H. Gjertsen, J. Sjoblom, H. Kallevik, and G. Oye. *Chemical influence on the formation, agglomeration, and natural transportability of gas hydrates. a multivariate component analysis.* Journal of Dispersion Science and Technology 2004;25:355–365.

[15] S. Hoiland, K. M. Askvik, P. Fotland, E. Alagic, T. Barth, and F. Fadnes. *Wettability of freon hydrates in crude oil/brine emulsions.* Journal of Colloid and Interface Science 2005;287:217–225.

[16] M. A. Kelland. *History of the development of low dosage hydrate inhibitors.* Energy & Fuels2006;20:825–847.

[17] P. V. Hemmingsen, X. Y. Li, J. L. Peytavy, and J. Sjoblom. *Hydrate plugging potential of original and modified crude oils.* Journal of Dispersion Science and Technology 2007;28:371–382.

[18] P. Muller and A. Saul. *Elastic effects on surface physics.* Surface Science Reports 2004;54(5-8):157–258.

[19] J. S. Rowlinson and B. Widom. *Molecular Theory of Capillarity*. International Series of Monographs on Chemistry. Clarendon Press, 1984.

[20] M. P. Gelfand and M. E. Fisher. *Finite size-effects in fluid interfaces.* Physica A 1990;166(1):1–74.

[21] R. L. Davidchack and B. B. Laird. Journal of Physical Chemistry B 2005;109:17802–17812.

[22] R. L. Davidchack, J. R. Morris, and B. B. Laird. *The anisotropic hard-sphere crystal-melt interfacial free energy from fluctuations.* Journal of Chemical Physics 2006;125(9).

[23] W. R. Fehlner and S. H. Vosko. *Product representation for cubic harmonics and special directions for determination of Fermi-surface and related properties.* Canadian Journal of Physics 1976;54(21):2159–2169.

[24] Bjørn Steen Sæthre, Alex C. Hoffmann, David van der Spoel, and Per Fotland. *Construction and validation of a molecular model for structure II clathrate hydrate.* submitted, 2008.

[25] HJC Berendsen, JPM Postma, WF van Gunsteren, A. Dinola, and JR Haak. *Molecular-dynamics with coupling to an external bath.* Journal of Chemical Physics 1984;81(8):3684–3690.

[26] S. Nose. *A molecular-dynamics method for simulations in the canonical ensemble.* Molecular Physics 1984;52(2):255–268.

[27] S. Senapati and M. L. Berkowitz. *Computer simulation study of the interface width of the liquid/liquid interface.* Physical Review Letters 2001;8717(17).

[28] D. Daan Frenkel. *Understanding molecular simulation : from algorithms to applications / Daan Frenkel, Berend Smit*. 2002.

[29] U. Essmann. *A smooth particle mesh Ewald method.* The Journal of Chemical Physics 1995;103(19):8577–8593. 0021-9606.

[30] S. Miyamoto and PA Kollmann. *SETTLE—an analytical version of the shake and rattle algorithm for rigid water models.* Journal of Computation Chemistry 1992;13(8):952–962.

[31] B. Hess, H. Bekker, H. J. C. Berendsen, and J. G. E. M. Fraaije. *LINCS: A linear constraint solver for molecular simulations.* Journal of Computational Chemistry 1997;18(12):1463–1472.